View metadata, citation and similar papers at core.ac.uk

brought to you by CORE

provided by Repository of Faculty of Science, University of Zagreb

PHYSICAL REVIEW B **80**, 245435 (2009)

Plasmonics in graphene at infrared frequencies

Marinko Jablan,[1,*] Hrvoje Buljan,[1,†] and Marin Soljačić[2,‡]

[1]*Department of Physics, University of Zagreb, Bijenička c. 32, 10000 Zagreb, Croatia*

[2]*Department of Physics, Massachusetts Institute of Technology, 77 Massachusetts Avenue, Cambridge, Massachusetts 02139, USA*

(Received 30 September 2009; published 23 December 2009)

We point out that plasmons in doped graphene simultaneously enable low losses and significant wave localization for frequencies below that of the optical phonon branch $\hbar\omega_{Oph}\approx 0.2$ eV. Large plasmon losses occur in the interband regime (via excitation of electron-hole pairs), which can be pushed toward higher frequencies for higher-doping values. For sufficiently large dopings, there is a bandwidth of frequencies from ω_{Oph} up to the interband threshold, where a plasmon decay channel via emission of an optical phonon together with an electron-hole pair is nonegligible. The calculation of losses is performed within the framework of a random-phase approximation and number conserving relaxation-time approximation. The measured DC relaxation-time serves as an input parameter characterizing collisions with impurities, whereas the contribution from optical phonons is estimated from the influence of the electron-phonon coupling on the optical conductivity. Optical properties of plasmons in graphene are in many relevant aspects similar to optical properties of surface plasmons propagating on dielectric-metal interface, which have been drawing a lot of interest lately because of their importance for nanophotonics. Therefore, the fact that plasmons in graphene could have low losses for certain frequencies makes them potentially interesting for nanophotonic applications.

DOI: 10.1103/PhysRevB.80.245435 PACS number(s): 73.20.Mf, 73.25.+i

I. INTRODUCTION

In recent years, an enormous interest has been surrounding the field of plasmonics, because of the variety of tremendously exciting and novel phenomena it could enable. On one hand, plasmonics seems to be the only viable path toward realization of nanophotonics: control of light at scales substantially smaller than the wavelength.[1–4] On the other hand, plasmonics is a crucial ingredient for implementation of most metamaterials, and thereby all the exciting phenomena that they support,[5–8] including negative refraction, superlensing, and cloaking. However, there is one large and so far insurmountable obstacle toward achieving this great vision: plasmonic materials (most notably metals) have enormous losses in the frequency regimes of interest. This greatly motivates us to explore plasmons and their losses in a newly available material with unique properties: graphene.[9–15]

Graphene is a single two-dimensional (2D) plane of carbon atoms arranged in a honeycomb lattice, which has only recently been demonstrated in high-quality samples and with superior mobilities.[9–15] This material is a zero-gap semiconductor, which can be doped to high values of electron or hole concentrations by applying voltage externally,[9] much like in field effect transistors (FET). While this kind of control over electrical properties of materials is at the heart of modern electronics, it was also demonstrated that the same procedure (electric gating)[16,17] leads to a dramatic change in optical properties of graphene because of its impact on the strong interband transitions. Collective excitations (plasmons) in graphene hold potential for technological applications as well;[18–27] for example, coherent terahertz sources based on plasmon amplification were suggested and discussed in Refs. 19 and 20. Graphene was predicted to support a transverse electric (TE) mode,[23] which is not present in usual 2D systems with parabolic electron dispersion. Thermoplasma polaritons in graphene have been discussed in Ref. 18, pointing out at new opportunities in the field of plasmonics.

Here, we investigate plasmons in doped graphene and demonstrate that they simultaneously enable low losses and significant wave localization for frequencies of the light smaller than the optical phonon frequency $\hbar\omega_{Oph}\approx 0.2$ eV.[28] Interband losses via emission of electron-hole pairs (first-order process) can be blocked by sufficiently increasing the doping level, which pushes the interband threshold frequency ω_{inter} toward higher values (already experimentally achieved doping levels can push it even up to near infrared frequencies). The plasmon decay channel via emission of an optical phonon together with an electron-hole pair (second-order process) is inactive for $\omega<\omega_{Oph}$ (due to energy conservation), however, for frequencies larger than ω_{Oph} this decay channel is non-negligible. This is particularly important for large enough doping values when the interband threshold ω_{inter} is above ω_{Oph}: in the interval $\omega_{Oph}<\omega<\omega_{\text{inter}}$ the first-order process is suppressed, but the phonon decay channel is open. In this article, the calculation of losses is performed within the framework of a random-phase approximation (RPA) and number conserving relaxation-time (RT) approximation;[29] the measured DC relaxation-time from Ref. 9 serves as an input parameter characterizing collisions with impurities, whereas the optical phonon relaxation times are estimated from the influence of the electron-phonon coupling[30] on the optical conductivity.[31]

In Sec. II, we provide a brief review of conventional surface plasmons and their relevance for nanophotonics. In Sec. III, we discuss the trade off between plasmon losses and wave localization in doped graphene, as well as the optical properties of these plasmons. We conclude and provide an outlook in Sec. IV.

II. SURFACE PLASMONS

Surface plasmons (SPs) are electromagnetic (EM) waves that propagate along the boundary surface of a metal and a

 ©2009 The American Physical Society

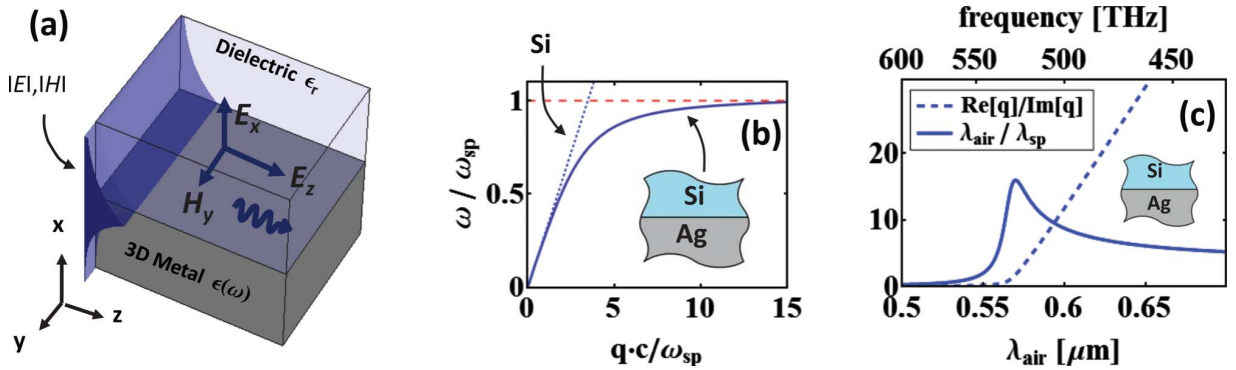

FIG. 1. (Color online) (a) Schematic description of a surface plasmon (SP) on metal-dielectric interface. (b) SP dispersion curve (solid blue line) for Ag-Si interfaces; dotted blue is the light line in Si; dashed red line denotes the SP resonance. (c) Wave localization and propagation length for SPs at Ag-Si interface (experimental Ag losses are taken into account).

dielectric [see Fig. 1(a)]; these are transverse magnetic (TM) modes accompanied by collective oscillations of surface charges, which decay exponentially in the transverse directions (see, e.g., Refs. 1 and 2 and references therein). Their dispersion curve is given by

$$q_{\mathrm{sp}} = \frac{\omega}{c}\sqrt{\frac{\epsilon_r \epsilon(\omega)}{\epsilon_r + \epsilon(\omega)}} \tag{1}$$

[see Fig. 1(b)]; note that close to the SP resonance ($\omega = \omega_{SP}$), the SP wave vector [solid blue line in Fig. 1(b)] is much larger than the wave vector of the same frequency excitation in the bulk dielectric [dotted blue line in Fig. 1(b)]. As a result, a localized SP wave packet can be much smaller than a same frequency wave packet in a dielectric. Moreover, this "shrinkage" is accompanied by a large transverse localization of the plasmonic modes. These features are considered very promising for enabling nanophotonics,[1–4] as well as high field localization and enhancement. A necessary condition for the existence of SPs is $\epsilon(\omega) < -\epsilon_r$ (i.e., $\epsilon(\omega)$ is negative), which is why metals are usually used. However, SPs in metals are known to have small propagation lengths, which are conveniently quantified (in terms of the SP wavelength) with the ratio $\Re q_{\mathrm{sp}}/\Im q_{\mathrm{sp}}$; this quantity is a measure of how many SP wavelengths can an SP propagate before it loses most of its energy. The wave localization (or wave "shrinkage") is quantified as $\lambda_{\mathrm{air}}/\lambda_{\mathrm{sp}}$, where $\lambda_{\mathrm{air}} = 2\pi c/\omega$ (the wavelength in air). These quantities are plotted in Fig. 1(c) for the case of Ag-Si interface, by using experimental data (see Ref. 3 and references therein) to model silver (metal with the lowest losses for the frequencies of interest). Near the SP resonance, wave localization reaches its peak; however, losses are very high there resulting in a small propagation length $l \approx 0.1\lambda_{\mathrm{sp}} \approx 5$ nm. At higher wavelengths one can achieve low losses but at the expense of poor wave localization.

III. PLASMONS AND THEIR LOSSES IN DOPED GRAPHENE

Graphene behaves as an essentially 2D electronic system. In the absence of doping, conduction and valence bands meet at a point (called Dirac point) which is also the position of the Fermi energy. The band structure, calculated in the tight binding approximation is shown in Fig. 2(b) (see Ref. 25 and references therein); for low energies the dispersion around the Dirac point can be expressed as $E_{n,\mathbf{k}} = n v_F \hbar |\mathbf{k}|$, where the Fermi velocity is $v_F = 10^6$ m/s, $n = 1$ for conduction, and $n = -1$ for the valence band. Recent experiments[32] have shown that this linear dispersion relation is still valid even up to the energies (frequencies) of visible light, which includes the regime we are interested in.

Here, we consider TM modes in geometry depicted in Fig. 2(a), where graphene is surrounded with dielectrics of constants ϵ_{r1} and ϵ_{r2}. Throughout the paper, for definiteness we use $\epsilon_{r1} = 4$ corresponding to SiO_2 substrate, and $\epsilon_{r2} = 1$ for air on top of graphene, which corresponds to a typical experimental setup. TM modes are found by assuming that the electric field has the form

$$\begin{aligned} &E_z = Ae^{iqz - Q_1 x}, \quad E_y = 0, \quad E_x = Be^{iqz - Q_1 x}, \quad \text{for } x > 0, \\ &E_z = Ce^{iqz + Q_2 x}, \quad E_y = 0, \quad E_x = De^{iqz + Q_2 x}, \quad \text{for } x < 0. \end{aligned} \tag{2}$$

After inserting this ansatz into Maxwell's equations and matching the boundary conditions [which include the conductance of the 2D graphene layer, $\sigma(\omega, q)$], we obtain the dispersion relation for TM modes:

$$\frac{\epsilon_{r1}}{\sqrt{q^2 - \frac{\epsilon_{r1}\omega^2}{c^2}}} + \frac{\epsilon_{r2}}{\sqrt{q^2 - \frac{\epsilon_{r2}\omega^2}{c^2}}} = -\frac{\sigma(\omega, q) i}{\omega \epsilon_0}. \tag{3}$$

By explicitly writing the dependence of the conductivity on the wave vector q we allow for the possibility of nonlocal effects, where the mean free path of electrons can be smaller than q^{-1}.[33] Throughout this work, we consider the nonretarded regime ($q \gg \omega/c$), so Eq. (3) simplifies to

$$q \approx Q_1 \approx Q_2 \approx \epsilon_0 \frac{\epsilon_{r1} + \epsilon_{r2}}{2} \frac{2i\omega}{\sigma(\omega, q)}. \tag{4}$$

Note that a small wavelength (large q) leads to a high transversal localization of the modes, which are also accompanied by a collective surface charge oscillation, similar to SPs in metals; however, it should be understood that, in contrast to

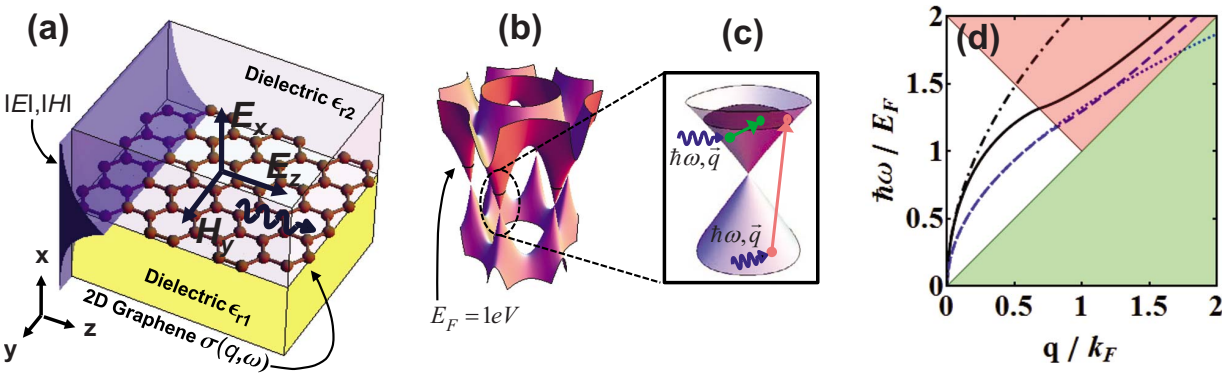

FIG. 2. (Color online) (a) Schematic of the graphene system and TM plasmon modes. Note that the profile of the fields looks the same as the fields of an SP [Fig. 1(a)]. (b) Electronic band structure of graphene; to indicate the vertical scale we show the Fermi energy level for the case $E_F=1$ eV. (c) Sketch of the intraband (green arrows) and interband (red arrows) single particle excitations that can lead to large losses; these losses can be avoided by implementing a sufficiently high doping. (d) Plasmon RPA and semiclassical dispersion curves. Black solid (RPA) and black dot-dashed (semiclassical) lines correspond to $\epsilon_{r1}=\epsilon_{r2}=1$; Blue dashed (RPA) and blue dotted (semiclassical) lines correspond to $\epsilon_{r1}=4$ and $\epsilon_{r2}=1$. The green (lower) and rose (upper) shaded areas represent regimes of intraband and interband excitations, respectively.

SPs, here we deal with 2D collective excitations, i.e., plasmons. We note that even though field profiles of plasmons in graphene and SPs in metals look the same, these two systems are qualitatively different since electrons in graphene are essentially frozen in the transverse dimension.[34] This fact and the differences in electronic dispersions (linear Dirac cones vs. usual parabolic) lead to qualitatively different dispersions of TM modes in these two systems [see Fig. 1(b) and 2(d)]. To find dispersion of plasmons in graphene we need the conductivity of graphene $\sigma(\omega,q)$, which we now proceed to analyze by employing the semiclassical model[33] (in Sec. III A), RPA and number conserving relaxation-time approximation[29] (in Sec. III B), and by estimating the relaxation-time due to the influence of electron-phonon coupling[30] on the optical conductivity[31] (in Sec. III C).

A. Semiclassical model

For the sake of the clarity of the presentation, we first note that by employing a simple semiclassical model for the conductivity (see Ref. 33), one obtains a Drude-like expression:[35]

$$\sigma(\omega) = \frac{e^2 E_F}{\pi\hbar^2}\frac{i}{\omega + i\tau^{-1}} \tag{5}$$

(the semiclassical conductivity does not depend on q). Here τ denotes the RT, which in a phenomenological way takes into account losses due to electron impurity, electron defect, and electron-phonon scattering. Equation (5) is obtained by assuming zero temperature $T\approx 0$, which is a good approximation for highly doped graphene considered here, since $E_F \gg k_B T$. From Eqs. (4) and (5) it is straightforward to obtain plasmon dispersion relation:

$$q(\omega) = \frac{\pi\hbar^2\epsilon_0(\epsilon_{r1}+\epsilon_{r2})}{e^2 E_F}\left(1+\frac{i}{\tau\omega}\right)\omega^2, \tag{6}$$

as well as losses,

$$\frac{\Re q}{\Im q} = \omega\tau = \frac{2\pi c\tau}{\lambda_{\text{air}}}. \tag{7}$$

In order to quantify losses one should estimate the relaxation time τ. If the frequency ω is below the interband threshold frequency ω_{inter}, and if $\omega < \omega_{Oph}$, then both interband damping and plasmon decay via excitation of an optical phonon together with an electron-hole pair are inactive. In this case, the relaxation time can be estimated from DC measurements,[9,13] i.e., it can be identified with DC relaxation time, which arises mainly from impurities (see Refs. 9 and 13). It is reasonable to expect that impurity related relaxation time will not display large frequency dependence. In order to gain insight into the losses by using this line of reasoning let us assume that the doping level is given by $E_F=0.64$ eV (corresponding to electron concentration of $n=3\times 10^{13}$ cm^{-2}); the relaxation time corresponds to DC mobility $\mu=10000$ cm^2/Vs measured in Ref. 9: $\tau_{DC}=\mu\hbar\sqrt{n\pi}/ev_F=6.4\times 10^{-13}$ s. As an example, for the frequency $\hbar\omega=0.155$ eV ($\lambda_{\text{air}}=8$ μm), the semiclassical model yields $\Re q/\Im q\approx 151$ for losses and $\lambda_{\text{air}}/\lambda_p\approx 42$ for wave localization. Note that both of these numbers are quite favorable compared to conventional SPs [e.g., see Fig. 1(c)]. It will be shown in the sequel that for the doping value $E_F=0.64$ eV this frequency is below the interband loss threshold, and it is evidently also smaller than the optical phonon loss threshold $\hbar\omega_{Oph}\approx 0.2$ eV, so both of these loss mechanisms can indeed be neglected.

B. RPA and relaxation-time approximation

In order to take the interband losses into account, we use the self-consistent linear response theory, also known as the RPA,[33] together with the relaxation-time (finite τ) approximation introduced by Mermin.[29] Both of these approaches, that is, the collisionless RPA ($\tau\to\infty$),[21,22] and the RPA-RT approximation (finite τ),[20] have been applied to study graphene. In the $\tau\to\infty$ case, the RPA 2D polarizability of graphene is given by:[22]

$$\chi(q,\omega) = \frac{e^2}{q^2}\Pi(q,\omega), \tag{8}$$

where

$$\Pi(q,\omega) = \frac{4}{\Omega}\sum_{\mathbf{k},n_1,n_2}\frac{f(E_{n_2,\mathbf{k}+\mathbf{q}}) - f(E_{n_1,\mathbf{k}})}{\hbar\omega + E_{n_1,\mathbf{k}} - E_{n_2,\mathbf{k}+\mathbf{q}}} \times |\langle n_1,\mathbf{k}|e^{-i\mathbf{q}\cdot\mathbf{r}}|n_2,\mathbf{k}+\mathbf{q}\rangle|^2. \tag{9}$$

Here, $f(E)=(e^{(E-E_F)/k_BT}+1)^{-1}$ is the Fermi distribution function, E_F is the Fermi energy and factor 4 stands for 2 spin and 2 valley degeneracies. Note that in Eq. (8) ω is given an infinitesimally small imaginary part which leads to the famous Landau damping; that is, plasmons can decay by exciting an electron-hole pair (interband and intraband scattering) as illustrated in Fig. 2(c). The effects of other types of scattering (impurities, phonons) can be accounted for by using the relaxation-time τ as a parameter within the RPA-RT approach,[29] which takes into account conservation of local electron number. Within this approximation the 2D polarizability is

$$\chi_\tau(q,\omega) = \frac{(1+i/\omega\tau)\chi(q,\omega+i/\tau)}{1+(i/\omega\tau)\chi(q,\omega+i/\tau)/\chi(q,0)}. \tag{10}$$

The 2D dielectric function and conductivity are respectively given by (see Ref. 36):

$$\epsilon_{\mathrm{RPA}}(q,\omega) = \frac{\epsilon_{r1}+\epsilon_{r2}}{2} + \frac{q}{2\epsilon_0}\chi_\tau(q,\omega), \tag{11}$$

and

$$\sigma_{\mathrm{RPA}}(q,\omega) = -i\omega\chi_\tau(q,\omega). \tag{12}$$

We note here that throughout the text only π—bands are taken into consideration; it is known that in graphite, higher σ—bands give rise to a small background dielectric constant[37] at low energies, which is straightforward to implement in the formalism. Using Eqs. (4) and (12) we obtain that the properties of plasmons (i.e., dispersion, wave localization and losses) can be calculated by solving

$$\epsilon_{\mathrm{RPA}}(q,\omega) = 0, \tag{13}$$

with complex wave vector $q=q_1+iq_2$. The calculation is simplified by linearizing Eq. (13) in terms of small q_2/q_1, to obtain,

$$\frac{\epsilon_{r1}+\epsilon_{r2}}{2} + \frac{e^2}{2\epsilon_0 q_1}\Re[\Pi(q_1,\omega)] = 0, \tag{14}$$

for the plasmon dispersion, and

$$q_2 = \frac{\Im[\Pi(q_1,\omega)] + \frac{1}{\tau}\frac{\partial}{\partial\omega}\Re[\Pi(q_1,\omega)] + \frac{1}{\omega\tau}\Re\{\Pi(q_1,\omega)[1-\Pi(q_1,\omega)/\Pi(q_1,0)]\}}{\frac{1}{q_1}\Re[\Pi(q_1,\omega)] - \frac{\partial}{\partial q_1}\Re[\Pi(q_1,\omega)]} \tag{15}$$

yielding losses. Note that in the lowest order, the dispersion relation (and consequently $\lambda_{\mathrm{air}}/\lambda_p$ and the group velocity v_g) does not depend on τ. This linearization is valid when $q_2 \ll q_1$; as the plasmon losses increase, e.g., after entering the interband regime [the rose area in Fig. 2(d)], results from Eqs. (14) and (15) should be regarded as only qualitative. The characteristic shape of the plasmon dispersion is shown in Fig. 2(d). Note that the semiclassical model and the RPA model agree well if the system is sufficiently below the interband threshold [for small q, $\omega(q)\sim\sqrt{q}$ as in Eq. (6)]. By comparing Figs. 2(d) and 1(b) we see that the dispersion for SPs on silver-dielectric surface qualitatively differs from the plasmon dispersion in graphene.[34] While SPs' dispersion relation approaches an asymptote ($\omega\to\omega_{SP}$) for large q values [Eq. (1)], graphene plasmon relation gives $\omega(q)$ which continuously increases [Fig. 2(d)].

Theoretically predicted plasmon losses $\Re q/\Im q$ and wave localization $\lambda_{\mathrm{air}}/\lambda_p$ are illustrated in Fig. 3 for doping level $E_F=0.135$ eV and relaxation time $\tau=1.35\times10^{-13}$ s. We observe that for this particular doping level, for wavelengths smaller than $\lambda_{\mathrm{inter}}\approx 7.7$ μm, the system is in the regime of high interband losses (rose shaded region). Below the interband threshold, both losses and wave localization obtained by employing RPA-RT approach are quite well described by the previously obtained semiclassical formulas. Since the frequencies below the interband threshold are (for the assumed doping level) also below the optical phonon frequency, the relaxation time can be estimated from DC measurements.

At this point we also note that in all our calculations we have neglected the finite temperature effects, i.e., $T\approx 0$. To justify this, we note that for doping values utilized in this paper the Fermi energies are 0.135 eV $\approx 5.2k_BT_r$ ($n=1.35\times10^{12}$ cm^{-2}) and 0.64 eV $\approx 25k_BT_r$ ($n=3\times10^{13}$ cm^{-2}) for room temperature $T_r=300$ K. The effect of finite temperature is to slightly smear the sharpness of the interband threshold, but only in the vicinity ($\sim k_BT_r$) of the threshold.

By increasing the doping, E_F increases, and the region of interband plasmonic losses moves toward higher frequencies (smaller wavelengths). However, by increasing the doping,

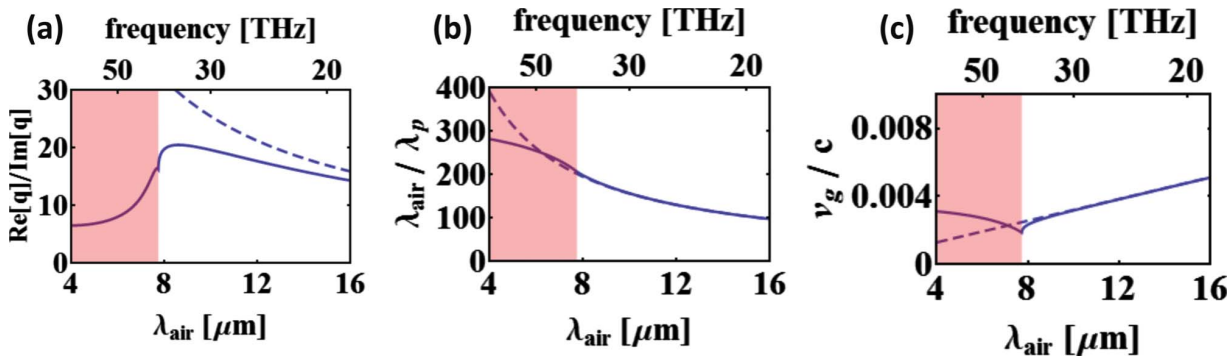

FIG. 3. (Color online) Properties of plasmons in doped graphene. Solid-lines are obtained with the number-conserving RPA calculation, and the dashed lines with the semiclassical approach. Losses (a), field localization (wave "shrinkage") (b), and group velocity (c) for doping $E_F=0.135$ eV, and relaxation time $\tau=1.35\times10^{-13}$ s, which corresponds to the mobility of 10 000 $\mathrm{cm}^2/\mathrm{Vs}$. The upper scale in all figures is frequency $\nu=\omega/2\pi$, whereas the rose shaded areas denote the region of high-interband losses.

the interband threshold frequency will eventually become larger than graphene's optical phonon frequency ω_{Oph}: there will exist an interval of frequencies, $\omega_{Oph}<\omega<\omega_{\mathrm{inter}}$, where it is kinematically possible for the photon of frequency ω to excite an electron-hole pair together with emission of an optical phonon. This second-order process can reduce the relaxation time estimated from DC measurements and should be taken into account, as we show in the following subsection.

C. Losses due to optical phonons

In what follows, we estimate and discuss the relaxation time due to the electron-phonon coupling. This can be done by using the Kubo formula which has been utilized in Ref. 31 to calculate the real part of the optical conductivity, $\Re\sigma(\omega,q=0)$. The calculation of conductivity $\Re\sigma(\omega,0)$ involves the electron self-energy $\Sigma(E)$, whose imaginary part expresses the width of a state with energy E, whereas the real part corresponds to the energy shift. Let us assume that the electron self-energy stems from the electron-phonon coupling and impurities,

$$\Sigma(E)=\Sigma_{e-ph}(E)+\Sigma_{\mathrm{imp}}(E). \tag{16}$$

For Σ_{e-ph} we utilize a simple yet fairly accurate model derived in Ref. 30: if $|E-E_F|>\hbar\omega_{Oph}$, then

$$\Im\Sigma_{e-ph}(E)=\gamma|E-\mathrm{sgn}(E-E_F)\hbar\omega_{Oph}|, \tag{17}$$

while elsewhere $\Im\Sigma_{e-ph}(E)=0$; the dimensionless constant $\gamma=18.3\times10^{-3}$ (Ref. 30) is proportional to the square of the electron-phonon matrix element,[30] i.e., the electron-phonon coupling coefficient. In order to mimic impurities, we will assume that $\Im\Sigma_{\mathrm{imp}}(E)$ is a constant (whose value can be estimated from DC measurements). The real parts of the self-energies are calculated by employing the Kramers-Krönig relations. In all our calculations the cutoff energy is taken to be 8.4 eV, which corresponds to the cutoff wave-vector $k_c=\pi/a$, where $a=2.46$ Å. By employing these self-energies we calculate the conductivity $\Re\sigma(\omega,q=0)$, from which we estimate the relaxation time by using Eq. (5), i.e.,

$$\tau(\omega)\approx\frac{e^2E_F}{\pi\hbar^2\omega^2}\frac{1}{\Re\sigma(\omega,0)} \tag{18}$$

for the region below the interband threshold; in deriving Eq. (18) we have assumed $\tau\omega\gg1$.

Figure 4 plots the real part of the conductivity and the relaxation time for two values of doping: $E_F=0.135$ eV ($n=1.35\times10^{12}$ cm^{-2}, solid line) and $E_F=0.64$ eV ($n=3\times10^{13}$ cm^{-2}, dashed line). In order to isolate the influence of the electron-phonon coupling on the conductivity and plasmon losses, the contribution from impurities is assumed to be very small: $\Im\Sigma_{\mathrm{imp}}(E)=10^{-6}$ eV. The real part of the conductivity has a universal value $\sigma_0=\pi e^2/2h$ above the interband threshold value $\hbar\omega=2E_F$ (for $q=0$), e.g., see Refs. 17, 32, and 38. We clearly see that the relaxation time is not affected by the electron-phonon coupling for frequencies below ω_{Oph}, that is, we conclude that scattering from impurities and defects is a dominant decay mechanism for $\omega<\omega_{Oph}$ (assuming we operate below the interband threshold). However, for $\omega>\omega_{Oph}$, the relaxation times in Fig. 4 are on the

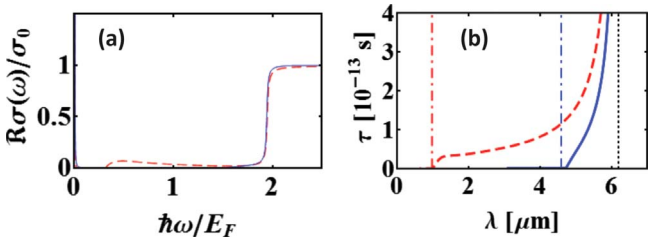

FIG. 4. (Color online) (a) The real part of the conductivity in units of $\sigma_0=\pi e^2/2h$ in dependence of frequency $\hbar\omega/E_F$, and (b) the corresponding relaxation time as a function of wavelength. The contribution to $\Re\sigma(\omega)$ from impurities is chosen to be negligible. The displayed graphs correspond to two different values of doping which yield $E_F=0.135$ eV (solid blue line), and $E_F=0.640$ eV (dashed red line). The position of the optical phonon frequency $\hbar\omega_{Oph}\approx0.2$ eV is depicted by the dotted vertical line in (b); dot-dashed lines depict the values of wavelengths corresponding to $2E_F$, that is, the interband threshold value (for $q=0$) for the two doping concentrations.

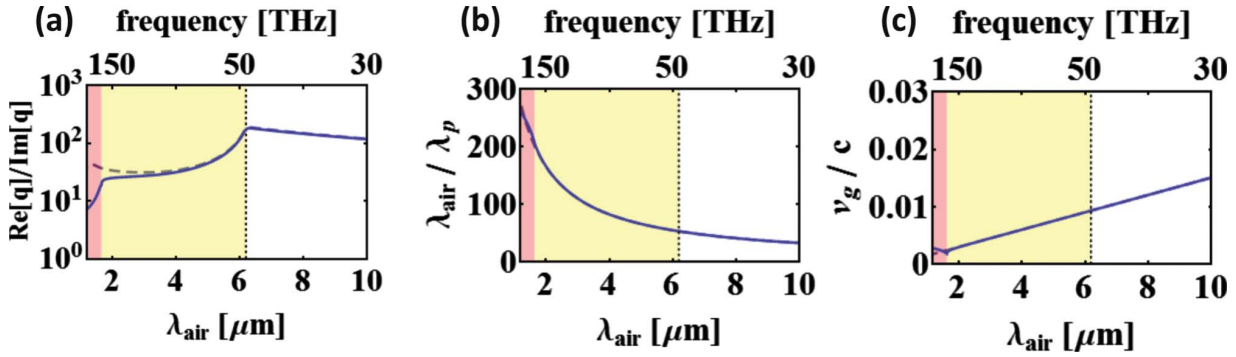

FIG. 5. (Color online) Properties of plasmons in doped graphene. Solid-lines are obtained with the number-conserving RPA calculation, and the dashed lines with the semiclassical approach. Losses (a), field localization (wave "shrinkage") (b), and group velocity (c) for doping $E_F=0.64$ eV; losses are calculated by using the relaxation time $\tau^{-1}=\tau_{DC}^{-1}+\tau_{e-ph}^{-1}$, where $\tau_{DC}=6.4\times10^{-13}$ s, and τ_{e-ph} is the relaxation time from the electron-phonon coupling for the given parameters. In the white regions (right regions in all panels), losses are determined by τ_{DC}. In the yellow shaded regions (central regions in all panels), losses are determined by the optical phonon emission, i.e., τ_{e-ph}. The rose shaded areas (left region in all panels) denote the region of high interband losses. Dotted vertical lines correspond to the optical phonon frequency $\omega_{Oph}\approx0.2$ eV. The upper scale in all figures is frequency $\nu=\omega/2\pi$. See text for details.

order of $10^{-14}-10^{-13}$ s, indicating that optical phonons are an important decay mechanism.

It should be emphasized that the exact calculated values should be taken with some reservation for the following reason: strictly speaking, one should calculate the relaxation times $\tau(\omega,q)$ along the plasmon dispersion curve given by Eq. (14); namely the matrix elements which enter the calculation depend on q, whereas the phase space available for the excitations also differ for $q=0$ and $q>0$. Moreover, the exact value of the matrix element for electron phonon coupling is still a matter of debate in the community (e.g., see Ref. 39). Therefore, the actual values for plasmon losses could be somewhat different for $\omega>\omega_{Oph}$. Nevertheless, fairly small values of relaxation times presented in Fig. 4 for $\omega>\omega_{Oph}$ indicate that emission of an optical phonon together with an electron-hole pair is an important decay mechanism in this regime. Precise calculations for $q>0$ and $\omega>\omega_{Oph}$ are a topic for a future paper.

Plasmonic losses and wave localization calculated from the RPA-RT approximation are illustrated in Fig. 5 for doping level $E_F=0.64$ eV and the relaxation time τ given by $\tau^{-1}=\tau_{DC}^{-1}+\tau_{e-ph}^{-1}$, where $\tau_{DC}=6.4\times10^{-13}$ s (mobility 10000 $\mathrm{cm}^2/\mathrm{Vs}$), whereas τ_{e-ph} is frequency dependent and corresponds to electron-phonon coupling assuming very clean samples [see dashed line in Fig. 4(b)]. Interband losses [left (rose shaded) regions in all panels] are active for wavelengths smaller than $\lambda_{\mathrm{inter}}\approx1.7$ μm. In the frequency interval $\omega_{\mathrm{inter}}>\omega>\omega_{Oph}$ [central (yellow shaded) regions in all panels], the decay mechanism via electron phonon coupling determines the loss rate, i.e., $\tau\approx\tau_{e-ph}$. For $\omega<\omega_{Oph}$ [right (white) regions in all panels], the DC relaxation time τ_{DC} can be used to estimate plasmon losses.

It should be noted that the mobility of 10000 $\mathrm{cm}^2/\mathrm{Vs}$ could be improved, likely even up to mobility 100 000 $\mathrm{cm}^2/\mathrm{Vs}$,[13] thereby further improving plasmon propagation lengths for frequencies below the optical phonon frequency. However, for these larger mobilities the calculation of losses should also include in more details the frequency dependent contribution to the relaxation time from acoustic phonons (this decay channel is open at all frequencies); such a calculation would not affect losses for $\omega>\omega_{Oph}$ where optical phonons are dominant.

IV. CONCLUSION AND OUTLOOK

In conclusion, we have used RPA and number-conserving relaxation-time approximation with experimentally available input parameters, and theoretical estimates for the relaxation-time utilizing electron-phonon coupling, to study plasmons and their losses in doped graphene. We have shown that for sufficiently large doping values high wave localization and low losses are simultaneously possible for frequencies below that of the optical phonon branch $\omega<\omega_{Oph}$ (i.e., $E_{\mathrm{plasmon}}<0.2$ eV). For sufficiently large doping values, there is an interval of frequencies above ω_{Oph} and below interband threshold, where an important decay mechanism for plasmons is excitation of an electron-hole pair together with an optical phonon (for $\omega<\omega_{Oph}$ this decay channel is inactive); the relaxation times for this channel were estimated and discussed. We point out that further more precise calculations of plasmon relaxation times should include coupling to the substrate (e.g., coupling to surface-plasmon polaritons of the substrate), a more precise shape of the phonon dispersion curves,[28] and dependence of the relaxation time via electron-phonon coupling on $q>0$ (see Sec. III C).

The main results, shown in Figs. 3 and 5 point out some intriguing opportunities offered by plasmons in graphene for the field of nanophotonics and metamaterials in infrared (i.e., for $\omega<\omega_{Oph}$). For example, we can see in those figures that high field localization and enhancement $\lambda_{\mathrm{air}}/\lambda_p\sim200$ [see Fig. 3(b)] are possible (resulting in $\lambda_p<50$ nm), while plasmons of this kind could have propagation loss-lengths as long as $\sim10\lambda_p$ [see Fig. 5(a)]; these values (albeit at different frequencies) are substantially more favorable than the corresponding values for conventional SPs, for example, for SPs at the Ag/Si interface $\lambda_{\mathrm{air}}/\lambda_p\sim20$, whereas propagation lengths are only $\sim0.1\lambda_{\mathrm{sp}}$ [see Fig. 1(c)]. Another interesting feature of plasmons in graphene is that, similar to usual

SP-systems,[4] wave localization is followed by a group velocity decrease; the group velocities can be of the order $v_g = 10^{-3} - 10^{-2}$ c, and the group velocity can be low over a wide frequency range, as depicted in Figs. 3(c) and 5(c). This is of interest for possible implementation of novel nonlinear optical devices in graphene, since it is known that small group velocities can lead to savings in both the device length and the operational power;[40] the latter would also be reduced because of the large transversal field localization of the plasmon modes.

ACKNOWLEDGMENTS

We would like to thank Leonid Levitov, J. D. Joannopoulos, Pablo Jarillo-Herrero, Tony Heinz, Vladimir Shalaev, Thomas Ebbesen, Ivan Kupčić, Antonio Šiber, Branko Gumhalter, Tobias Stauber, and Ivo Batistić, for many helpful comments. This work was supported in part by the Croatian Ministry of Science under Grant No. 119-0000000-1015. This work was also supported in part by the MRSEC program of National Science Foundation under Award No. DMR-0819762, in part by the U.S. Army Research Office through the institute of soldier nanotechnologies under Contract No. W911NF-07-D-0004, and also in part by the U.S. Department of Energy office of science, office of basic energy sciences, through S3TEC, which is a DOE energy frontier research center.

*mjablan@phy.hr
†hbuljan@phy.hr
‡soljacic@mit.edu

[1] W. L. Barnes, A. Dereux, and T. W. Ebbesen, Nature (London) **424**, 824 (2003).
[2] S. A. Maier and H. A. Atwater, J. Appl. Phys. **98**, 011101 (2005).
[3] S. Vedantam, H. Lee, J. Tang, J. Conway, M. Staffaroni, and E. Yablonovitch, Nano Lett. **9**, 3447 (2009).
[4] A. Karalis, E. Lidorikis, M. Ibanescu, J. D. Joannopoulos, and M. Soljačić, Phys. Rev. Lett. **95**, 063901 (2005).
[5] V. G. Veselago, Sov. Phys. Usp. **10**, 509 (1968).
[6] V. M. Shalaev, Nat. Photonics **1**, 41 (2007).
[7] J. B. Pendry, Phys. Rev. Lett. **85**, 3966 (2000).
[8] D. R. Smith, J. B. Pendry, and M. C. K. Wiltshire, Science **305**, 788 (2004).
[9] K. S. Novoselov, A. K. Geim, S. V. Morozov, D. Jiang, Y. Zhang, S. V. Dubonos, I. V. Grigorieva, and A. A. Firsov, Science **306**, 666 (2004).
[10] K. S. Novoselov, D. Jiang, F. Schedin, T. J. Booth, V. V. Khotkevich, S. V. Morozov, and A. K. Geim, Proc. Natl. Acad. Sci. U.S.A. **102**, 10451 (2005).
[11] K. S. Novoselov, A. K. Geim, S. V. Morozov, D. Jiang, M. I. Katsnelson, I. V. Grigorieva, S. V. Dubonos, and A. A. Firsov, Nature (London) **438**, 197 (2005).
[12] Y. Zhang, Y. W. Tan, H. L. Stormer, and P. Kim, Nature (London) **438**, 201 (2005).
[13] A. K. Geim and K. S. Novoselov, Nature Mater. **6**, 183 (2007).
[14] C. Berger, Z. Song, T. Li, X. Li, A. Y. Ogbazghi, R. Feng, Z. Dai, A. N. Marchenkov, E. H. Conrad, P. N. First, and W. A. de Heer, J. Phys. Chem. B **108**, 19912 (2004).
[15] C. Berger, Z. Song, X. Li, X. Wu, N. Brown, C. Naud, D. Mayou, T. Li, J. Hass, A. N. Marchenkov, E. H. Conrad, P. N. First, and W. A. de Heer, Science **312**, 1191 (2006).
[16] F. Wang, Y. Zhang, Ch. Tian, C. Girit, Alex Zettl, M. Crommie, and Y. R. Shen, Science **320**, 206 (2008).
[17] Z. Q. Li, E. A. Henriksen, Z. Jiang, Z. Hao, M. C. Martin, P. Kim, H. L. Stormer, and D. N. Basov, Nat. Phys. **4**, 532 (2008).
[18] O. Vafek, Phys. Rev. Lett. **97**, 266406 (2006).
[19] V. Ryzhii, M. Ryzhii, and T. Otsuji, J. Appl. Phys. **101**, 083114 (2007).
[20] F. Rana, IEEE Trans. NanoTechnol. **7**, 91 (2008).
[21] B. Wunsch, T. Sauber, F. Sols, and F. Guinea, New J. Phys. **8**, 318 (2006).
[22] E. H. Hwang and S. Das Sarma, Phys. Rev. B **75**, 205418 (2007).
[23] S. A. Mikhailov and K. Ziegler, Phys. Rev. Lett. **99**, 016803 (2007).
[24] L. A. Falkovsky and S. S. Pershoguba, Phys. Rev. B **76**, 153410 (2007).
[25] A. Bostwick, T. Ohta, T. Seyller, K. Horn, and E. Rotenberg, Nat. Phys. **3**, 36 (2007).
[26] V. Ryzhii, A. Satou, and T. Otsuji, J. Appl. Phys. **101**, 024509 (2007).
[27] S. Gangadharaiah, A. M. Farid, and E. G. Mishchenko, Phys. Rev. Lett. **100**, 166802 (2008).
[28] For simplicity here we assume Einstein model for optical phonons, and assume that they form a branch at 0.2 eV. More precisely one should take into account that electrons interact with zone center phonons at $\hbar\Omega_\Gamma = 0.196$ eV (intravalley scattering) and zone boundary phonons at $\hbar\Omega_K = 0.161$ eV (intervalley scattering).
[29] N. D. Mermin, Phys. Rev. B **1**, 2362 (1970).
[30] Ch.-H. Park, F. Giustino, M. L. Cohen, and S. G. Louie, Phys. Rev. Lett. **99**, 086804 (2007).
[31] T. Stauber and N. M. R. Peres, J. Phys.: Condens. Matter **20**, 055002 (2008); see also T. Stauber, N. M. R. Peres, and A. H. Castro-Neto, Phys. Rev. B **78**, 085418 (2008).
[32] R. R. Nair, P. Blake, A. N. Grigorenko, K. S. Novoselov, T. J. Booth, T. Stauber, N. M. R. Peres, and A. K. Geim, Science **320**, 1308 (2008).
[33] N. W. Ashcroft and N. D. Mermin, *Solid State Physics* (Saunders, Philadelphia, PA, 1976).
[34] W. H. Backes, F. M. Peeters, F. Brosens, and J. T. Devreese, Phys. Rev. B **45**, 8437 (1992).
[35] G. W. Hanson, J. Appl. Phys. **104**, 084314 (2008).
[36] F. Stern, Phys. Rev. Lett. **18**, 546 (1967).
[37] E. A. Taft and H. R. Philipp, Phys. Rev. **138**, A197 (1965).
[38] K.-F. Mak, M. Y. Sfeir, Y. Wu, C.-H. Lui, J. A. Misewich, and T. F. Heinz, Phys. Rev. Lett. **101**, 196405 (2008).
[39] J. L. McChesney, A. Bostwick, T. Ohta, K. Emtsev, Th. Seyller, K. Horn, and E. Rotenberg, arXiv:0809.4046 (unpublished).
[40] M. Soljačić and J. D. Joannopoulos, Nature Mater. **3**, 211 (2004).